NUREG/CR-4972
ANL-87-27

Reactor Analysis and Safety Division

Reactor Analysis and Safety Division
Reactor Analysis and Safety Division

Two-Phase Flow Regime Transition Criteria in Post-Dryout Region Based on Flow Visualization Experiments

by N. T. Obot and M. Ishii

Argonne National Laboratory, Argonne, Illinois 60439
operated by The University of Chicago
Prepared for the Office of Nuclear Regulatory Research
U. S. Nuclear Regulatory Commission under Interagency Agreement DOE 40-550-75

8709030565 870630
PDR NUREG
CR-4972 R PDR

Argonne National Laboratory, with facilities in the states of Illinois and Idaho, is owned by the United States government, and operated by The University of Chicago under the provisions of a contract with the Department of Energy.

NOTICE

This report was prepared as an account of work sponsored by an agency of the United States Government. Neither the United States Government nor any agency thereof, or any of their employees, makes any warranty, expressed or implied, or assumes any legal liability or responsibility for any third party's use, or the results of such use, of any information, apparatus, product or process disclosed in this report, or represents that its use by such third party would not infringe privately owned rights.

Available from

Superintendent of Documents
U. S. Government Printing Office
Post Office Box 37082
Washington, D.C. 20013-7982

and

National Technical Information Service
Springfield, VA 22161

NUREG/CR-4972
ANL-87-27

(Distribution
Codes: R2
and R4)

ARGONNE NATIONAL LABORATORY
9700 South Cass Avenue
Argonne, Illinois 60439

TWO-PHASE FLOW REGIME TRANSITION CRITERIA IN POST-DRYOUT REGION BASED ON FLOW VISUALIZATION EXPERIMENTS

by

N. T. Obot* and M. Ishii

Reactor Analysis and Safety Division

Report Completed: June 1987

Report Issued: June 1987

Prepared for the Division of Accident Evaluation
Office of Nuclear Regulatory Research
U.S. Nuclear Regulatory Commission
Washington, D. C. 20555
under Interagency Agreement DOE 40-550-75

NRC FIN No. A2026

*Department of Chemical Engineering, Clarkson University, Potsdam, New York 13676.

TWO-PHASE FLOW REGIME TRANSITION CRITERIA IN POST-DRYOUT REGION BASED ON FLOW VISUALIZATION EXPERIMENTS

by

N. T. Obot and M. Ishii

ABSTRACT

A visual study of film boiling using photographic and high speed motion-picture methods was carried out to determine the flow regime transition criteria in the post-CHF region. An idealized inverted annular flow was obtained by introducing a liquid jet of Freon 113 through a nozzle, precisely centered with respect to the internal diameter of the test section, with an annular gas flow. The respective ranges for liquid and gas exit velocities were 0.05-0.5 and 0.03-7.9 m/s. Nitrogen and helium were used in the study.

For the present configuration, there are four basic flow regimes. Beginning from the nozzle exit, there is a smooth, inverted annular flow section with liquid in the core and gas in the annulus; followed by the rough wavy section with an intact liquid core, the agitated and the dispersed flow regimes. For a given liquid jet velocity, the axial extent of each flow regime decreases with increasing gas velocity through the annulus.

Generalized transition criteria and simplified correlations for the axial limits of the various flow regimes have been developed, by extending the results of previous studies on adiabatic inverted annular flow.

NRC FIN No.	Title
A2026	Phenomenological Modeling of Two-phase Flow in Water Reactor Safety Research

TABLE OF CONTENTS

LIST OF FIGURES

LIST OF TABLES

NOMENCLATURE

A_i	Constant, defined by Eq. (3)
B_i	Constant, defined by Eq. (4)
C_i	Constant, defined by Eq. (6)
Ca	Capillary number, $\mu_f v_f/\sigma_f$
D_j	Liquid jet hole diameter, m
L_B	Axial extent of a flow section, m
Re	Reynolds number, $\rho V D_j/\mu$
T	Temperature, °C
V	Velocity, m/s
V_{rel}	Relative velocity, $V_g - V_f$, m/s
We	Weber number, $\rho V^2 D_j/\sigma$
$We_{g,rel}$	Gas Weber number, $\rho_g V_{rel}^2 D_j/\sigma_f$

<u>Greek Symbols</u>

α	Void fraction at inlet to test section
μ	Viscosity, Pa.s
ρ	Density, kg/m^3
σ	Surface tension, N/m

<u>Subscripts</u>

f	Liquid
g	Gas
j	Liquid jet
rel	Relative, or based on V_{rel}

EXECUTIVE SUMMARY

An extensive experimental investigation of inverted annular flow was carried out with the objective of characterizing the various flow regimes. A flow visualization of a simplified film boiling geometry, consisting of a Freon 113 liquid jet surrounded by a gas annulus, was made. The parametric study included the effects of liquid and gas flow rates, gas species and inlet void fraction.

From the visual study, it has been determined that there are basically four flow regimes. Extending from the nozzle exit to as much as 20 nozzle diameters downstream, the flow is annular with liquid in the center and the gas in the annulus. Next, there is a rough wavy section; its dominant features being the presence of a fairly intact liquid core, not much different from that for the smooth section, and of nearly axisymmetric interfacial waves having wavelengths of about 10 mm (order of magnitude). Located immediately downstream of the rough wavy section, there is an agitated section where roll-wave entrainment and jet-induced instability predominate. Lastly, there is a dispersed ligaments/droplets flow regime which is confined to the downstream section near the exit of the test section. The axial limits of the flow regimes have been determined and these depend, to a marked extent, on the jet velocity and the relative velocity between the gas and the liquid.

Generalized transition criteria and simplified correlations of the axial extents of the various flow regimes have been developed and these indicate two trends; the existence of a relative velocity range over which the lengths are dependent only on liquid parameters, followed by a range for which there is a marked dependence on liquid and gas parameters, and void fraction. There are clear indications that the transition from the combined smooth and rough wavy sections to the agitated flow regime is governed by the same break-up mechanisms as for free liquid jets.

Droplets that were sheared off from the tops of the large amplitude roll waves as well as those originating from the rough surfaces of the agitated region were quite small, the maximum size being about 500 μm. However, the mean size for droplets in the dispersed region were considerably larger, being within 0.5-3 mm in diameter.

I. INTRODUCTION

An inverted annular flow, which consists of a liquid core surrounded by a vapor annulus (Fig. 1), is of considerable importance in the areas of LWR accident analysis, cryogenic heat transfer, and other confined, low quality film boiling applications. Although extensive studies of the heat transfer characteristics for this flow situation have been carried out by numerous researchers [1-3], there have been very few systematic investigations of the hydrodynamics of inverted annular flow. Presumably, the limited information on the hydrodynamics of the post CHF region reflects two things. First, such experiments are usually difficult to design and this is further complicated by the fact that conventional flow measurement techniques are not suitable for film boiling studies. And, secondly, they are expensive, often requiring sophisticated instrumentation including facilities for photographic and/or high speed motion picture studies. This lack of information on the general features of this flow field often results in unsatisfactory analysis of many film boiling applications.

An understanding of the effects of the various parameters on the prevailing local flow conditions in the post CHF region (such as, the shape of the liquid/vapor interface, the stability as well as the disintegration of liquid core) is of fundamental importance in flow modeling and development of predictive equations for interfacial transfer rates. Realizing that in typical film boiling experiments, control of test conditions as well as direct measurements of the pertinent flow parameters, that would be needed for such an understanding, are quite difficult, the recourse must be to devise simplified experiments.

The main objective of the inverted annular flow research program was to determine the effects of inlet liquid and gas conditions on the flow regimes in the post CHF region. A flow visualization of a simplified film boiling configuration, consisting of a Freon 113 liquid core surrounded by a gas annulus, was made. From an analysis of the still photographs and high speed motion pictures, it was determined that there are basically four flow regimes and it was also possible to determine the axial extents of these flow zones with remarkable consistency. Predictive equations, in generalized and simplified forms, were then developed for the axial limits of the different flow regimes.

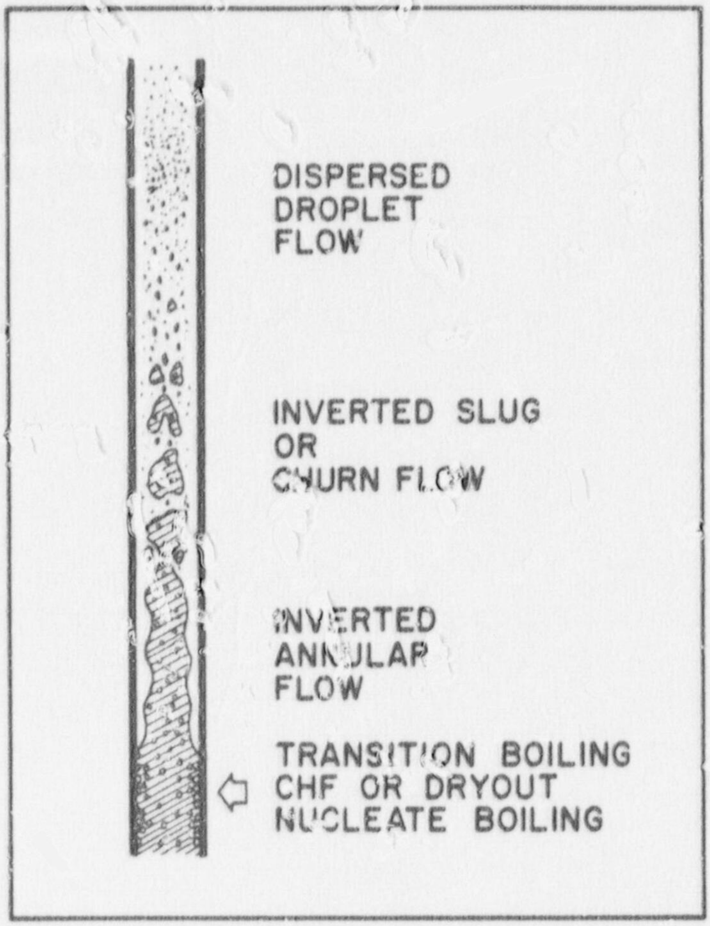

Fig. 1. Possible Flow Regimes in Post Dryout Region

II. REVIEW OF EXPERIMENTAL STUDIES OF POST-CHF REGION

Most of the research on post CHF region dealt mainly with heat transfer. Excellent reviews of the widespread literature were provided by Jordan [1] and Clemments and Colver [2]. A subsequent review by Kalinin et al. [3] considered both free and forced convective film boiling in great detail. Complete tabulations as well as extensive graphical comparisons of the various predictive equations for heat transfer were given. However, because heat transfer or hydraulic resistance is significantly influenced by the regime of film boiling, some of the disagreement among the various correlations are not so readily explained due to insufficient understanding of the complex hydrodynamics of the post CHF region.

The present state of knowledge of the structure and mechanisms of film boiling derives primarily from visual and high-speed motion picture observations. For external horizontal surfaces, still photographs and motion pictures taken by Westwater and Santangelo [4] showed a viscous-like flow pattern in which small ripples caused only slight disturbance of the liquid-vapor interface. Similar studies with vertical external surfaces have been carried out by numerous researchers (Hsu and Westwater [5,6], Coury and Dukler [7]; to mention but a few). The series of still photographs of Hsu and Westwater indicated the presence of wavy motion, the waves themselves being neither regular nor sharply defined. The magnitudes of the interfacial deformations were found to be more pronounced for vertical than horizontal tubes, with similar effects on heat transfer. Accordingly, Hsu and Westwater concluded that film boiling outside of a vertical tube was far superior to that with horizontal tubes.

Coury and Dukler measured interfacial wave characteristics, instantaneous and time-averaged rates of heat transfer. They concluded that the fluctuations in surface temperature were driven by the action of large interfacial waves of low frequency. Subcooling was found to diminish the interfacial oscillations.

Visual and high-speed motion picture observations of film boiling in channels have been reported by a number of researchers. For example, Chi and co-workers [8-10] considered film boiling of saturated hydrogen under transient cooling conditions and obtained the following flow regimes along the horizontal test section: annular, slug and dispersed flows. For the range of flow conditions covered in their study, Kalinin et al. [11] observed both the annular and slug flow regimes.

For upward flow of liquid nitrogen in a vertical tube, Laverty and Rohsenow [12] obtained two distinct flow regimes: an annular flow with liquid in the center and vapor in the annulus occurred at the beginning of the heated section, followed by a dispersed region of filaments/droplets of liquids at greater tube lengths. In a subsequent study, Forslund and Rohsenow [13] confirmed the large departure from thermal equilibrium in the dispersed flow film boiling. They made measurements of the droplet size at the exit of the test section, from which it was concluded that the droplet breakup process along the tube was governed by the critical Weber number criterion; the Weber number being defined in terms of the relative velocity between the gas and the liquid, vapor/gas density, droplet diameter and liquid surface tension.

A detailed experimental study of adiabatic inverted annular flow was carried out by DeJarlais [14], DeJarlais et al. [15], and Ishii and DeJarlais [16] using coaxial downward flow water jets and various gases in a glass tube. The disintegration of the liquid core into droplets was found to be due to two different mechanisms: wave instabilities at the interface and roll-wave entrainment. Correlations for core shape, breakup mechanisms and dispersed core drop size were developed, by extending the results of free jet instability, roll-wave entrainment and churn turbulent droplet stability studies.

Since the absence of film boiling conditions (no wall wetting, droplet vaporization in the vicinity of heated wall, etc.) may limit the applicability of the adiabatic results, an extensive and consistent flow visualization study of a diabatic inverted annular flow was performed by DeJarlais [17] and Ishii and DeJarlais [18,19]. A simplified upward flow geometry, consisting of a liquid jet of Freon 113 surrounded by a gas annulus, was studied. In addition to the existence of an annular and dispersed flow regime, in line with the results of Laverty and Rohsenow [12], the presence of two well-defined regimes - the agitated and the inverted slug/churn flow, was also documented. The axial extent of each flow regime, as well as the transition from one regime to another, was found to depend markedly on the relative velocity between the gas and the liquid, in agreement with the observation of Laverty and Rohsenow. No correlations were developed for the extents of the flow regimes.

The channel flow film boiling studies reviewed so far dealt almost exclusively with visual, still and movie-camera observations of the complete structure of the two-phase flow field. Although it has long been known that the prevailing film boiling regime has profound effects on heat transfer and on the hydraulic resistance, only several studies of film boiling hydraulic resistance have been reported (Kalinin et al. [11], and Graham et al. [20]). Also, there is almost no systematic study of the rather complicated void fraction distribution for film boiling in channels for a range of inlet flow conditions. Ottosen [21] obtained void fraction data using γ-ray adsorption technique in the flow visualization experiments in a vertical glass tube with liquid nitrogen as a coolant. He noted that the transition from an annular to a dispersed flow occurred at void fractions in excess of 80% at atmospheric pressure. Kurilenko et al. [22] made measurements of void fraction by radioisotope method using vertical and downward flow transient quenching of a steel tube with liquid nitrogen, but the scope of the study was quite limited.

Although some progress has been made in the identification of the various flow regimes, as reflected here by the findings of previous investigators, the general state of knowledge of the detailed structure and mechanisms of two-phase flows for film boiling has not been entirely satisfactory. Comprehensive experimental investigations of these complex hydrodynamics of the post CHF region are certainly needed in order to provide data for further development of theoretical models.

Although the emphasis in this review has been on the experimental studies, it should also be mentioned that a number of computer codes and analytical/empirical models have been developed for predictions of void fractions, wall temperatures and heat fluxes in the post-CHF region [23,24]. A review of the numerous analytical and empirical methods for annular and slug flow film boiling was carried out by Groeneveld [25] while Chen [26], in his review examined phenomenological questions relevant to our understanding of the transport mechanisms in the post-CHF heat transfer. More recently, Yadigaroglu and Bensalem [27] presented a critical and thorough review of the various approaches that are used for modeling of interfacial mass generation in two-phase flows, including a detailed discussion of the mechanistic models for inverted annular and dispersed flow film boiling. A common conclusion that can be inferred from these reviews amounted to this: there is need for experimental data base that would permit validation of the existing models as well as development of improved models.

III. EXPERIMENTAL FACILITY AND TEST PROCEDURES

Since very elaborate description of the apparatus and test procedures were given elsewhere [17-19], these will be briefly summarized here, with no exhaustive details.

A. Test Apparatus

The steady state film boiling experimental facility, shown schematically in Fig. 2, consisted of a transparent quartz tube, a simplified inverted annular flow geometry formed by a round liquid jet core surrounded by an

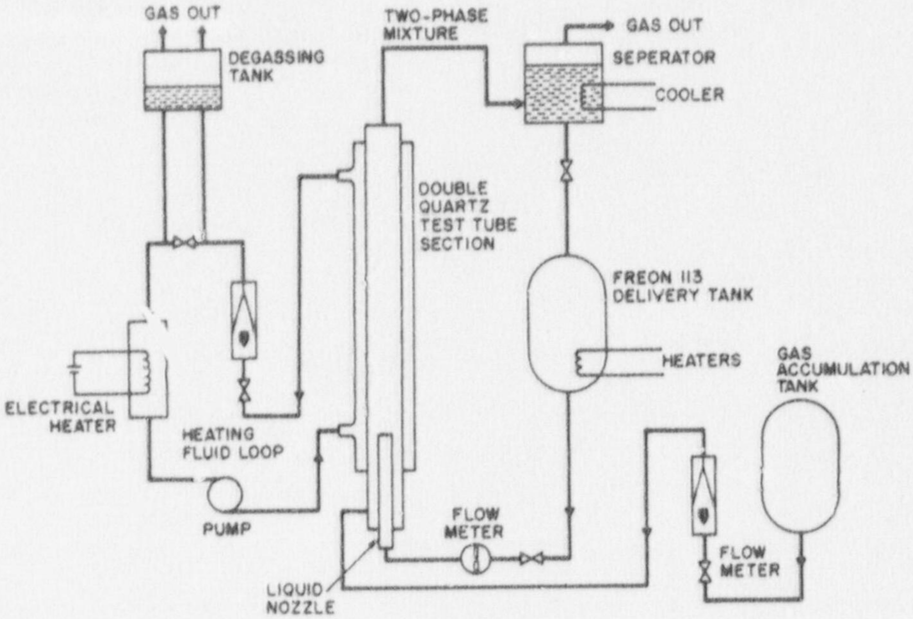

Fig. 2. Schematic of the Experimental Facility

annular gas flow. The liquid jet of Freon-113 was discharged into the test section using thin-walled interchangeable stainless steel tubes (9.02 and 10.8 mm, ID), each of which was precisely centered with respect to the internal diameter of the heated quartz tube, while the gas (nitrogen or helium) was introduced via the annular gap between the stainless steel nozzle and the quartz tube. The corresponding void fractions were 0.56 and 0.37 for D_j = 9.02 and 10.8 mm, respectively. Liquid and gas flow rates were measured with turbine flowmeter and rotameters, respectively; temperatures at all critical locations being sensed with chromel-alumel thermocouples.

The heated portion of the test sections, 1.0 m in length (Fig. 3), consisted of two quartz tubes, finished in much the same way as Liebig or West condensers. The dimensions of the inner and outer quartz tubes were 16 x 13.6 mm OD/ID and 35 x 31 mm OD/ID, respectively, giving an annular gap of 31 x 16 mm OD/ID through which a high temperature heat transfer fluid (Syltherm 80 by Dow Corning) was circulated. The inner quartz tube extended beyond the outer one to give an unheated entrance length of 150 mm (Fig. 3).

Inverted annular flow could be established in the test section by heating the heat transfer fluid above minimum film boiling temperature and then introducing saturated or subcooled test liquids such as Freon-113 into the inner

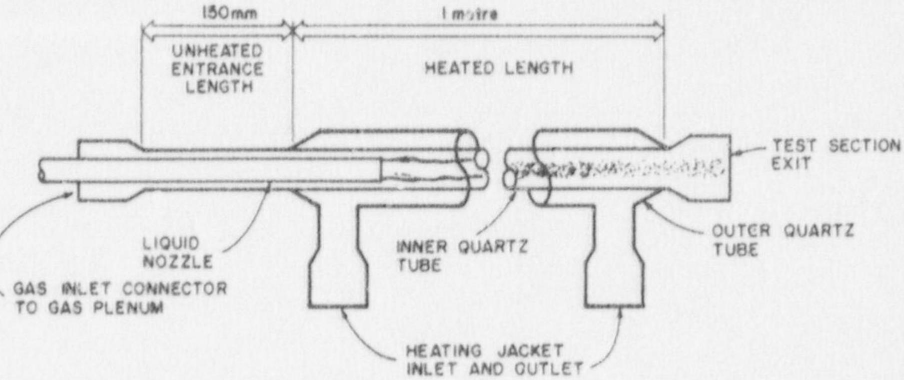

Fig. 3. Details of the Test Section

tube directly. The drawback with this approach is one of lack of control of the annular gas conditions. The alternative simplified inverted annular flow geometry, one that was used for the present study and afforded accurate control of the flow conditions at the inlet to the test section, was obtained by introducing a circular liquid jet through the stainless steel tube with a surrounding annular gas flow (Figs. 2 and 3), the latter being discharged through an annular plenum located below the quartz test section.

B. Test Procedures and Photographic Technique

Preliminary preparations prior to a trial run included degassing of the freon supply tank and the establishment of the desired freon temperature by heating and/or cooling, charging of the gas accumulation tank to 60-80 psig, heating of the Syltherm loop to a stable temperature of 225-270°C, cooling of the separator tank (used to recover the freon from a two phase mixture leaving the test section) to about 0°C or lower, and a check on the lighting conditions to be used for photographic and/or motion picture observations.

During a trial run, visualization of the hydrodynamic behavior within the test section was accomplished using both still photograph and high speed motion pictures. For the former, a 35 mm SLR camera was used along with 400 ASA black and white film. Lighting was provided by either of two 3 μs strobe lights, each delivering a 0.5 w-s pulse of light. With this short exposure time, small (0.1 mm) droplets traveling at speeds above 10 m/s were observed without significant blurring of the image. The light from the strobe was bounced off a white background onto the test section.

For a given test run, a series of still photographs were taken using a 55 mm lens which provided a complete view of a 0.3 m length of the test section on each 35 mm film frame. The pictures were taken at five or six locations, spanning the full length of the test section, including the entrance and exit sections. At each location, two to five photographs were taken, giving about 10-30 frames for each trial. To obtain more detailed structure of the flow field, additional still photographs were taken with 105 mm or 200 mm lenses. Either back or side strobe lighting was used.

For some selected trials, motion pictures were taken using several different cameras and Kodak VNX 430 (400 ASA) color reversal film, with a film speed of 500 fps for most trials. Lighting was provided by four 450W flood lights, these being directed onto the same background as noted above for the still photographs. The interested reader may wish to refer to the detailed discussion of the qualification methods for optical and/or photographic techniques which is given in [17].

IV. ANALYSIS AND DISCUSSION OF RESULTS

In this section, a brief overview of the hydrodynamics of the flow field is given, followed by a discussion of the predictive equations for the axial extents of the different flow regions. Also, selected data for drop sizes in the agitated and dispersed flow regions are presented and discussed.

A relevant comment here deals with the data used to generate the correlations shown subsequently. These were obtained by analyzing the still photographs, taken with the 35 mm black and white film, in the following manner. The extent of the different flow regions were established by carefully studying the developed negatives using a light table fitted with binocular microscope, the reference scale being the image of the graduated scale (in cm) mounted alongside the test section. For drop size analysis, the negatives obtained with the 55 mm SLR lens were projected onto a screen, with a minimum negative-to-screen image magnification of 500. By this procedure the drop sizes were determined down to the 100-200 mm size range. Although determination of the flow regime or the sizes of the droplets were accomplished with little difficulty, a shortcoming is the rather time consuming frame by frame analysis. Motion pictures of the flow field were analyzed on a motion picture analyzer, with x-y plotting cross hairs and film projection speeds from 48 fps down to zero.

A. An Overview of the Hydrodynamics of the Flow Field

Prior to presentation and discussion of the results for the axial extent of the flow regimes, it is instructive to review the flow patterns that were established for this simplified inverted annular flow. Since a more detailed discussion of the general features as well as extensive photographic illustrations are contained in DeJarlais and Ishii [17], this brief summary is intended to provide the reader with a clear picture of the most important characteristics of the various flow regimes, and will not contain exhaustive details.

1. Smooth (Small Surface Wave) Section

This smooth region begins from the nozzle exit and can extend to about thirty nozzle diameters depending, of course, on the relative velocity between the gas and the liquid core. For a given liquid jet exit velocity, the maximum length occurs at very low gas exit velocities, decreasing markedly with increasing gas velocity to almost zero at high gas velocities. The shearing effect on the liquid jet by the gas; notably, the complete elimination of a smooth section as observed in the present study at high gas velocities, parallels that usually encountered in twin fluid atomization processes.

2. Rough Wavy Section

With increasing distance downstream, the liquid interface becomes wavy with nearly symmetric waves, the wavelengths of which are roughly 10 mm (order of magnitude). Except for the existence of a rough wavy interface, this region of the flow field is quite solid, with a fairly intact liquid core filling the center of the test section. As with the smooth section, its axial extent varies according to whether the gas velocity is greater or less than the liquid jet velocity. For example, with V_{rel} (i.e., V_g-V_f) > 0, the physical length of this flow regime decreases (from about 10-20 nozzle diameters) with increasing V_{rel} to the point that, at a V_{rel} of about 2 m/s, both the smooth and rough wavy sections are nonexistent, the prevailing regimes being an agitated zone in the immediate vicinity of the nozzle exit and large liquid slugs/ligaments over the remaining portion of the test section. By contrast, test trials with $V_{rel} < 0$ resulted in lengths that were within 10-50 jet hole diameters. It is pertinent to note that in DeJarlais and Ishii [17], also [18,19], this regime is referred to as the agitated solid core while the present agitated section, to be discussed next, corresponds to the inverted slug/churn flow in [17-19].

3. Agitated Section

With increasing downstream distance and/or at sufficiently high gas velocity, the nearly axisymmetric interfacial waves become very irregular and transform to large amplitude or roll waves. Farther from the rough wavy section or at a still larger gas velocity, significant interfacial deformation occurs, resulting in the break-up of portions of the roll-waves into ligaments and droplets. This mechanism of liquid break-up or drop formation has been treated quite well by Ishii and Grolmes [28] and DeJarlais [14], hence the details will not be given here. Other general features of this flow regime include the formation of skirt-like annular sheets of liquid due to extreme growth and distortion of the roll-waves, the presence of highly agitated liquid annulus in the vicinity of the heated wall and of large liquid slugs in the central portion of the test section. With these general characteristics, it is quite clear that, unlike the smooth or rough wavy section, this section of the flow which may extend beyond the end of the heated portion of the test section (depending on the liquid and gas flow rates, see Table A.IV of the appendix) is very unstable.

4. Dispersed (Ligament and Drop) Section

For the ranges of liquid and gas velocities covered in the present study, this flow regime was generally confined to the downstream locations nearest to the test section exit. For test trials with high relative velocities, i.e., $(V_g - V_f) > 1$ m/s, the dominant feature of the downstream flow field was that of dispersed ligaments/droplets with either of the gas species. For low-to-moderate V_{rel} values, many of the large liquid ligaments or slugs at the exit of the test section were very much distorted. If the test section were sufficiently long, it is likely that these ligaments would eventually disintegrate into smaller, stable drops.

B. Predictive Equations for the Axial Extent of Flow Regimes

1. Formulation of the Generalized Correlations

From a detailed study of an adiabatic inverted annular flow [14-16], it was established conclusively that the correlated jet break-up data followed two distinct trends; one for the region over which the jet break-up length was independent of void fraction, relative velocity or gas density, with a marked sensitivity of the break-up to these variables for the second region. The break-up lengths for these two regions were closely approximated by the following equations:

$$L_B/D_j = 480\ Re_j^{-0.53}\ We_j^{0.5} \tag{1}$$

$$L_B/D_j = 685\ Re_j^{-0.53}\ We_j^{0.5}\ [We_{g,rel}/\alpha^2]^{-0.645} \tag{2}$$

Since the two curves intersect at $We_{g,rel}/\alpha^2 = 1.73$, this critical value of the modified Weber number provides a useful criterion for determining the validity range for each equation. Another important finding was that the break-up mechanisms for an adiabatic inverted annular flow were similar to those documented in the literature for free jets.

On the basis of the above information, it was envisaged that the maximum extent of each flow regime could be correlated in terms of the nondimensional variables in Eqs. (1) and (2). Accordingly, the present data were reduced and the results are presented graphically in Figs. 4-7. The first three figures show, successively, the upper bound to the range of axial extents for the smooth, rough wavy and agitated flow sections. Beyond the agitated flow regime lies the dispersed ligaments/droplets section. The extent of this zone is shown in Fig. 7 from which it may be noted that it extends beyond the heated portion of the test section for most trials. The data used to prepare these plots are also presented in tabular form in Table A.IV of the appendix.

In each of Figs. 4-7, data are shown for the two gas species (helium and nitrogen) tested. To provide useful insight on the role of relative velocity, it was considered worthwhile to further identify the data points in Figs. 4-6 according to whether the average gas velocity at the annulus (V_g) is less or greater than the liquid jet velocity (V_f) at the inlet to the test section.

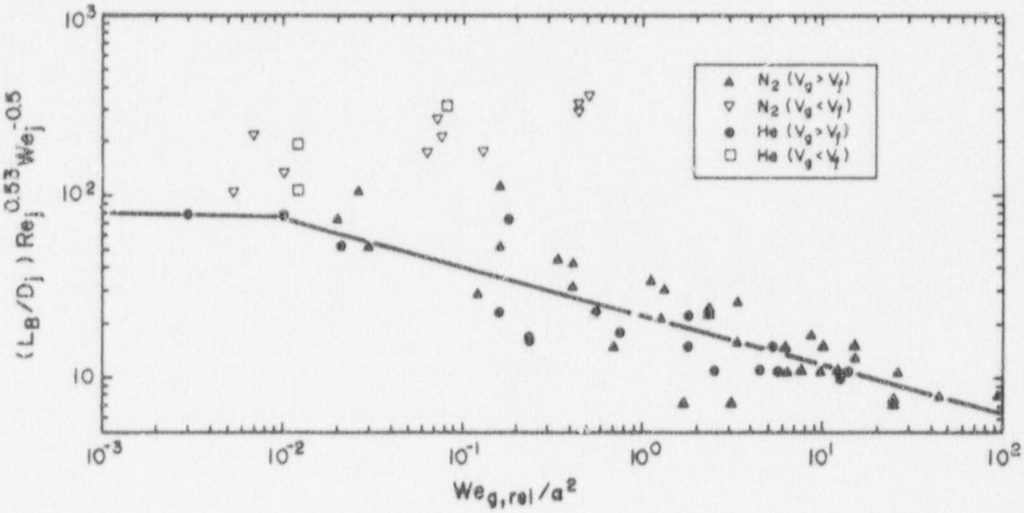

Fig. 4. Correlation for Upper Limit of Smooth Flow Section

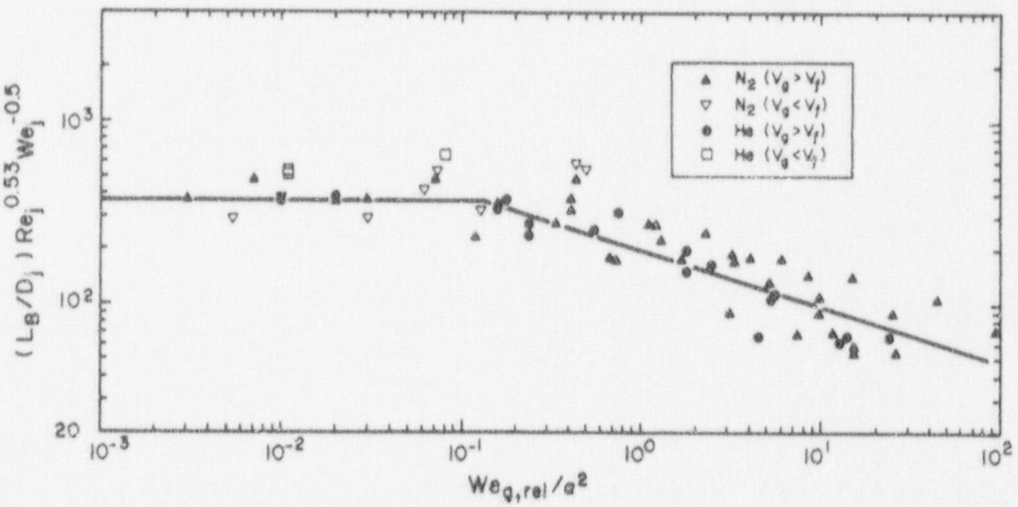

Fig. 5. Correlation for Upper Limit of Rough Wavy Section

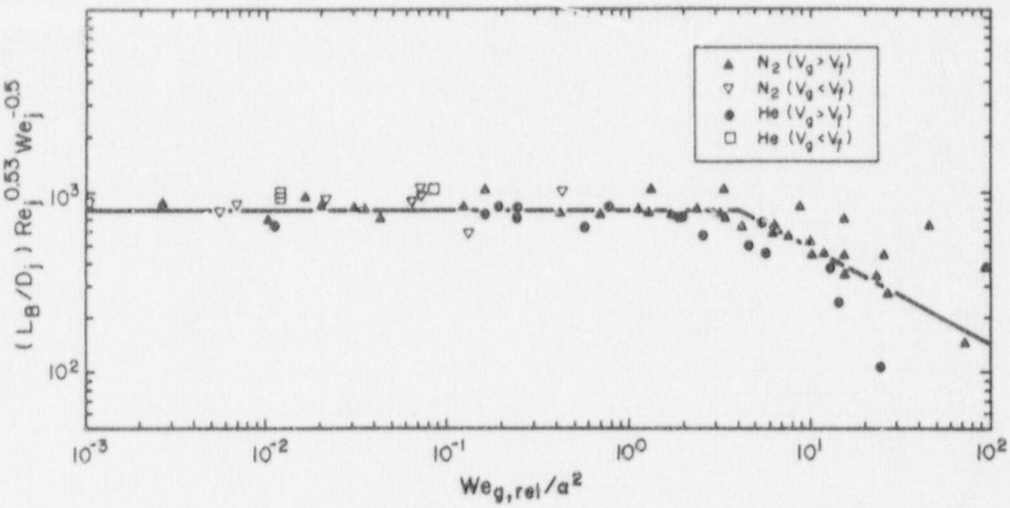

Fig. 6. Correlation for Upper Limit of Agitated Section

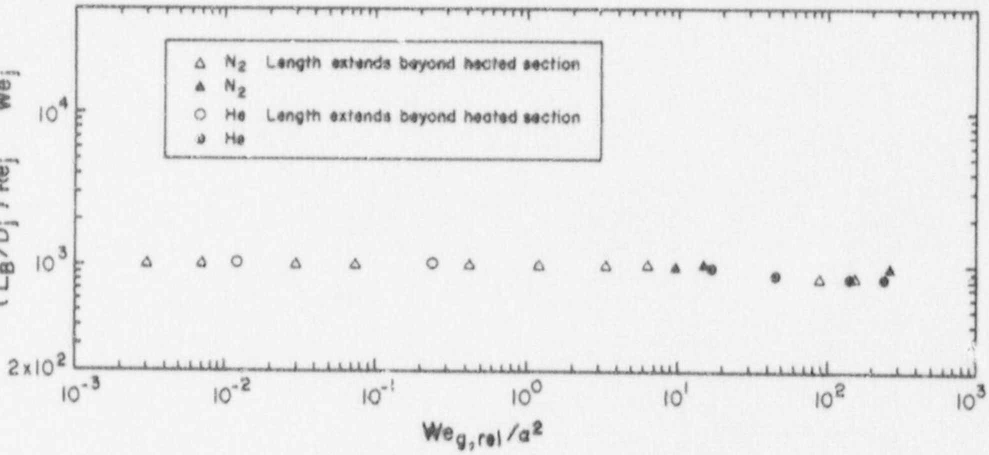

Fig. 7. Typical Extent of Dispersed Flow Section

Another general comment, one that is of particular importance, relates to the interpretation of the data for L_B/D_j. Each value of L_B, always measured from the nozzle exit, is scaled with the constant nozzle diameter, D_j. Thus, depending on the liquid and gas velocity, the observed maximum length, L_B/D_j, for the rough wavy section includes that for the smooth region, while that for the agitated regime may include both the smooth and rough wavy regions. Likewise, the L_B/D_j value for the dispersed zone may encompass all or some of those for the preceding upstream regimes.

The general trends on Figs. 4-7 are twofold; a nearly constant L_B/D_j value with increasing $We_{g,rel}/\alpha^2$ for the region over which the maximum limits depend solely on the inlet liquid jet conditions, Re_j and We_j, followed by steadily decreasing values with further increases in $We_{g,rel}/\alpha^2$, which is the expected trend when L_B/D_j is dependent on both liquid and gas conditions at the inlet to the test section. For the smooth section, the length of which exhibits the greatest sensitivity to variations in relative velocity, gas density and void fraction, the few data available for $We_{g,rel}/\alpha^2 < 10^{-3}$ together with those shown in Fig. 4 favor the observation that this extent is essentially independent of gas Weber number for $We_{g,rel}/\alpha^2 < 10^{-2}$.

An exception to the trends noted above is observed to occur for the dispersed flow section (Fig. 7). Here, it will be noted that, over the entire $10^{-3} \leq We_{g,rel}/\alpha^2 \leq 10^3$ range, L_B/D_j is almost determined solely by the liquid jet Reynolds and Weber numbers, Re_j and We_j. Conceivably, with increasing modified gas Weber number conditions would eventually have been obtained for which L_B/D_j would decrease markedly with $We_{g,rel}/\alpha^2$, in line with the trends on Figs. 4-6. The general trend on this figure appears to support this view.

A closer examination of the results in Figs. 4-6 reveals one consistent trend with test trials for which the liquid jet velocities were larger than the annular gas velocities at the inlet to the test section. It may be noted that, for the smooth, rough wavy or agitated section, the axial limits for $V_f > V_g$ tend to lie above the mean regression line determined for data with $V_f < V_g$; notably for the range of $We_{g,rel}/\alpha^2$ over which L_B/D_j is only susceptible to liquid conditions. It may also be noted that the above trend is most pronounced for the smooth section, with vestiges in the rough wavy and agitated regions. The clear implication here is that viewing the results in terms of the absolute values of relative velocity does not provide a very accurate picture of the axial limits of the flow regimes.

Over the range where L_B/D_j is independent of $We_{g,rel}/\alpha^2$, a linear regression using only data for $V_f < V_g$ resulted in relations of the form:

$$L_B/D_j \lesssim A_i \, Re_j^{-0.53} \, We_j^{0.5} \tag{3}$$

The numerical values of constant, A_i, together with the approximate ranges of validity of Eq. (3) are summarized in Table I. From comparison of the A_i

Table I. Summary of Predictive Equations

Flow Section	First Region+		Second Region+		
	$L_B/D_j \lesseqgtr A_i\ Re_j^{-0.53}\ We_j^{0.5}$		$L_B/D_j \le B_i\ Re_j^{-0.53}\ We_j^{0.5}\ [We_{g,rel}/\alpha^2]^{m_i}$		
	A_i	Validity range for $We_{g,rel}/\alpha^2$	B_i	m_i	Range for $We_{g,rel}/\alpha^2$
Smooth	< 80	$\le 10^{-2}$	25	-0.27	$>10^{-2}$
Rough Wavy	<380	$\le 10^{-1}$	200	-0.31	$>10^{-1}$
Agitated	<770	≤ 3.5	1500	-0.5	>3.5
Dispersed	>770	≤ 10	-	-	

+Range for Re_j and We_j: $1775 \le Re_j \le 13{,}280$ and $4.5 \le We_j \le 260$.

values in Table I with the value in Eq. (1), i.e., $A_i = 480$, which was developed from adiabatic tests based on the break-up mechanism of free liquid jets, it is quite apparent that Eq. (1) would predict lengths that are somewhat higher than, but not significantly different from, the combined lengths determined here for the smooth and rough wavy sections.

When L_B/D_j depends on $We_{g,rel}/\alpha^2$, the data are approximated by:

$$L_B/D_j \le B_i \, Re_j^{-0.53} \, We_j^{0.5} \, [We_{g,rel}/\alpha^2]^{m_i} \tag{4}$$

The appropriate values for B_i, m_i along with the ranges of validity are also given in Table I. The values for B_i and m_i were determined by logarithmic least squares technique and the correlation coefficients were between 0.85 and 0.9, these being as good as can be expected for carefully run experiments using a visual analysis for flow regime characterization; especially since replicate runs sometimes resulted in lengths that differed by as much as 100%. It may be noted that, for the constants A_i and B_i (Table I), the last digits have been rounded to zero or five and the error introduced by this procedure is less than one percent.

2. Simplified Correlations

The presentation in the preceding section is important in two respects. First, it provides good insight into the mechanisms that determine the axial extents of the various flow sections. And, second, good estimates of the critical gas Weber number for transition, from regions with no effect to those with marked dependence on relative velocity, can be established for nearly all of the flow sections.

For low-to-moderate gas velocities satisfying the conditions $V_g - V_f > 0$ and $L_B/D_j = f(Re_j, We_j)$, a further simplification of Eq. (3) can be made in order to provide predictive equations that may be readily applied for design calculations. Realizing that $We_j/Re_j = \mu_f V_f/\sigma_f$ (= Capillary number, Ca_j), Eq. (3) can be re-written as

$$(L_B/D_j)\, Re_j^{0.5}\, We_j^{-0.5} = (L_B/D_j)\, Ca^{-0.5} < A_i/Re_j^{0.03} \tag{5}$$

or

$$L_B/D_j \leq C_i(We_j/Re_j)^{1/2} \leq C_i\sqrt{Ca_j} \tag{6}$$

A straightforward re-analysis of the data for each trial was carried out by dividing the already computed values in Table A.IV by $Re_j^{0.03}$. For the $1,774 \leq Re_j \leq 13,279$ range covered in the present study, $Re_j^{0.03}$ varied from 1.252 to 1.330, with an average value which could be stated as 1.296±0.034, i.e., with about a 3% variation about the mean value. Although very good estimate of the constant C_i for each flow section can be obtained by simply dividing the appropriate value in Table I by 1.296, a linear regression using the new data set resulted in the following correlations:

$$\text{Smooth section:} \quad L_B/D_j \leq 60\sqrt{Ca_j}, \text{ for } (We_{g,rel}/\alpha^2) \leq 10^{-2} \tag{7}$$

$$\text{Rough wavy section:} \quad L_B/D_j \leq 295\sqrt{Ca_j}, \text{ for } (We_{g,rel}/\alpha^2) \leq 10^{-1} \tag{8}$$

$$\text{Agitated section:} \quad L_B/D_j \leq 595\sqrt{Ca_j}, \text{ for } (We_{g,rel}/\alpha^2) \leq 3.5 \tag{9}$$

$$\text{Dispersed section:} \quad L_B/D_j > 595\sqrt{Ca_j}, \text{ for } (We_{g,rel}/\alpha^2) \leq 10 \tag{10}$$

In addition to the individual ranges specified above, Eqs. (7)-(10) are valid for $0.0028 \leq Ca_j \leq 0.02$. As with Table I, the last digit is rounded to zero or 5. Equations (7)-(9) give estimates that are close to the values observed experimentally, with a 6-20% error band. As might be expected from the trend in Fig. 4, the largest percentage differences were calculated for the relatively short smooth section.

A final comment here deals with Eq. (10) which might appear at first to exclude the presence of a dispersed section over a third of the initial heated portion of the test section. Of the numerous trials with $V_{rel} \leq 2$ m/s, about 80% of the measured lengths satisfied Eq. (10). For all test trials with $V_{rel} > 2.0$ m/s, Eq. (10) did not apply. For instance, for the two nitrogen trials (#262, #296, Table A.IV of the appendix) with V_{rel} = 7.6 and 5.0 m/s, the onset of a dispersed ligament/droplet section was observed to occur at about 10-13 jet hole diameters downstream from the nozzle exit, which is considerably less than about 34 diameters that could be inferred from Eq. (10). This continual depletion of the liquid core into ligaments/droplets of liquid with increasing relative velocity, a generally expected trend, is qualitatively in agreement with the observations of Laverty and Rohsenow [12].

C. Droplet Generation and Drop Size Distributions

Downstream of the rough wavy section, a significant portion of the liquid surface area consists of small droplets formed by roll-wave entrainment and by jet instability within the agitation region. These droplets were quite small, with sizes under 200 μm in diameter. In the immediate vicinity of the heated wall, these small droplets were probably short-lived due to very rapid vaporization.

Typical size distributions for droplets formed by roll-wave entrainment and by instability at the rough surfaces of the agitated region are shown in Fig. 8 for three trials, two (708 and 727) with helium and the other with nitrogen. To obtain these data, photographs taken with the 200 mm lens (resolution down to roughly 25 μm, but limited depth of focus) focussed at the depth corresponding to the outer (facing) surface of the liquid nozzle were analyzed. With these focussing, droplets within 2-3 mm of the heated wall nearest to the camera were in sharp focus. Droplets observed shearing from roll-wave crests or within 10 mm of the leading (downstream) edges of the agitated masses were measured, provided they were within sharp focus, the others being ignored.

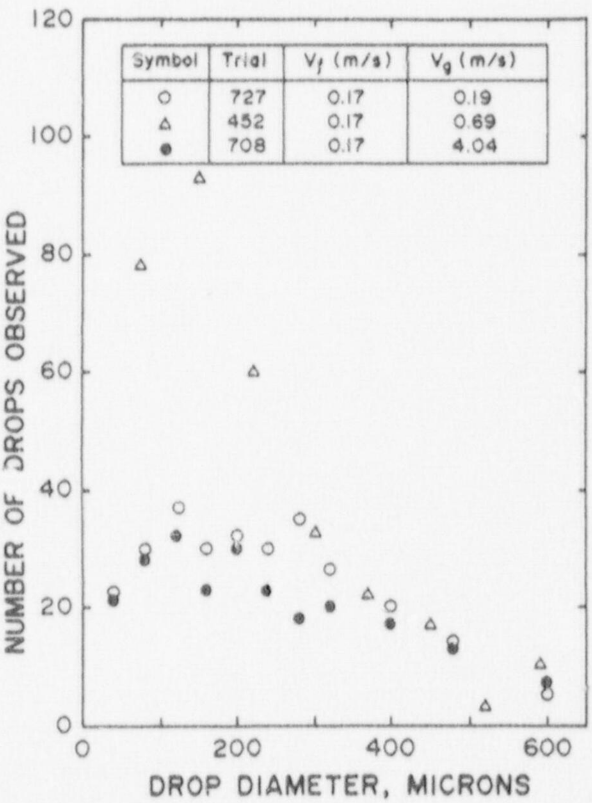

Fig. 8. Size Distribution for Droplets from Roll-wave/Agitated Surface

For high, positive relative velocities, the flow field near the exit of the test section is characterized by dispersed droplets, with unstable and distorted liquid ligaments/slugs for moderate relative velocities. These droplets are largely the result of roll-wave entrainment and jet instabilities, and the maximum drop size depends on the stability of the liquid core remnants and liquid mass in the agitated region. Typically, droplets/slugs over 3 mm were observed to be quite distorted and far from being spherical, a possible indication that these large drops (or small slugs) were unstable and would eventually disintegrate into smaller droplets in a sufficiently long test section.

Typical drop size distributions in the dispersed flow region are given in Fig. 9 for three trials, two (216 and 224) with nitrogen and the other with helium. These data were obtained by analyzing still photographs taken with the 55 mm lens (resolution down to about 100 μm). Spherical or near spherical droplets were recorded by diameter while unstable, distorted slugs were measured along long and short axes, and recorded by estimated total volume, assuming cylindrical form with the short axis corresponding to the diameter.

The following comment can be made about the results in Figs. 8 and 9. The maximum droplet size generated at the roll-wave crests/agitated surfaces as well as droplet size distributions in the dispersed film boiling regime should depend on the gas and liquid physical properties and on the relative velocity. In view of the rather complicated nature of the droplet size dependence on these parameters, combined with knowledge that smaller droplets are short-lived due to vaporization, no definite conclusions concerning these effects can be made from the limited information available.

V. SUMMARY AND CONCLUSIONS

A visualization study of a simplified film boiling flow geometry, consisting of a Freon 113 liquid jet surrounded by a gas annulus, was carried out with the objective of determining the various flow regimes. It has been established that the axial flow pattern for this model of an inverted annular flow consists basically of four regions; namely, a nearly smooth section which begins at the nozzle exit, a rough wavy section with an intact liquid core, an agitated and a dispersed flow regions, the latter being confined to the region

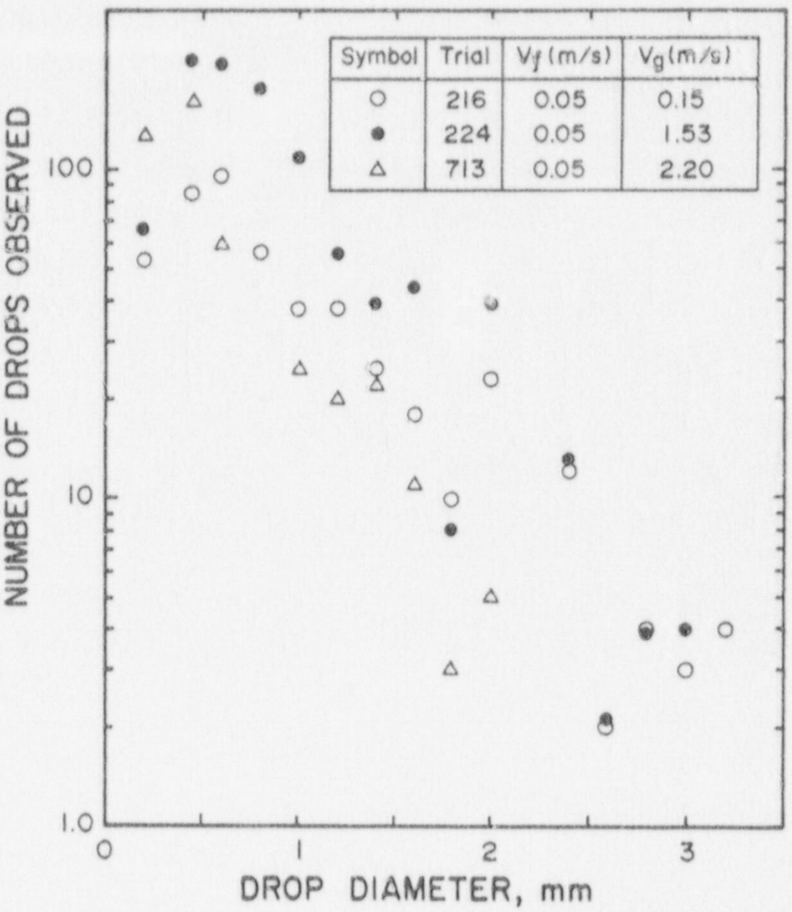

Fig. 9. Size Distribution for Droplets in the Dispersed Flow Regime

near the exit of the test section. The axial limits of these flow regimes depend markedly on the relative velocity between the gas and the liquid. The axial extent of each flow zone (L_B), expressed in terms of the liquid jet nozzle diameter (D_j) as L_B/D_j, has been correlated using the liquid jet Reynolds and Weber numbers (Re_j and We_j, respectively), and a modified gas Weber number based on relative velocity ($We_{g,rel}/\alpha^2$), where α is the void fraction.

For any particular flow regime, the proposed correlation follows two distinct trends, one for the $We_{g,rel}/\alpha^2$ range over which L_B/D_j depends only on the liquid jet parameters (Re_j and We_j) and the other for the region where L_B/D_j is a function of Re_j, We_j and $We_{g,rel}/\alpha^2$. For the former, the maximum extent of each flow regime is approximated by the relation:

$$L_B/D_j \lesssim A_i \, Re_j^{-0.53} \, We_j^{0.5}$$

where A_i is a constant, the numerical value of which is different for the different flow regimes. For adiabatic inverted annular flow, DeJarlais et al. [15] established that the nondimensional break-up length was adequately represented by the above equation with $A_i = 480$. However, from comparison of the present values of A_i with that noted above for the adiabatic case, it is concluded that the adiabatic equation will predict lengths that are 20-30% higher than the combined length determined here for the smooth and rough wavy sections.

With knowledge that $We_j/Re_j = \mu_f V_f/\sigma_f$ (= Capillary number, Ca_j), the desire to provide correlations that can be readily applied for design calculations prompted a further simplification of the above equation to the following form:

$$L_B/D_j \le C_i\sqrt{Ca_j}$$

where the constant, C_i, assumes values of 60, 380 and 595 for the smooth, rough wavy and agitated flow regimes, successively. Since the dispersed ligaments/droplets flow regime always lies downstream of the agitated section for low relative velocity, a close approximation of its extent is given by:

$$L_B/D_j > 595\sqrt{Ca_j}$$

Over the range of conditions for which L_B/D_j depends on the liquid jet parameters and the modified gas Weber number, the predictive equations are of the form:

$$L_B/D_j \le B_i\ Re_j^{-0.53}\ We_j^{0.5}\ [We_{g,rel}/\alpha^2]^{m_i}$$

where both B_i and m_i assume different values for the smooth, rough wavy and agitated regions. The general form of this equations, first proposed by DeJarlais et al. [15] for adiabatic inverted annular flow, was found to provide adequate representation of sinuous jet instability break-up at moderate interfacial shear, and roll-wave entrainment break-up at high interfacial shear. The present constants, B_i and m_i, are somewhat different from those established for an adiabatic study and the adiabatic equation gives L_B/D_j values that are almost double the combined length for the smooth and rough wavy sections.

Typical size distributions for droplets generated at the roll-wave crests (the maximum size being about 500 μm) as well as those formed in the dispersed flow regime (0.5-3 mm in diameter) have been presented.

ACKNOWLEDGMENTS

This work was performed under the auspices of the U.S. Nuclear Regulatory Commission. The authors would like to express their sincere appreciation to Drs. Richard Lee and Novak Zuber for valuable discussions and support on the subject.

REFERENCES

1. Jordan, D. P., "Film and Transition Boiling," Advances in Heat Transfer, Vol. 5, pp. 55-128 (1968).

2. Clemments, L. D. and Colver, C. P., "Natural Convection Film Boiling Heat Transfer," Ind. Eng. Chem., Vol. 62, #9, pp. 26-46 (1970).

3. Kalinin, E. K., Berlin, I. I., and Kostyuk, V. V., "Film-Boiling Heat Transfer," Advances in Heat Trans., Vol. 11, pp. 51-197 (1975).

4. Westwater, J. W. and Santangelo, J. C., "Photographic Study of Boiling," Ind. Eng. Chem., Vol. 47, #8, pp. 1605-1610 (1955).

5. Hsu, Y. Y. and Westwater, J. W., "Film Boiling from Vertical Tubes," AIChE J., Vol. 4, #1, pp. 58-62 (1958).

6. Hsu, Y. Y. and Westwater, J. W., "Approximate Theory for Film Boiling on Vertical Surfaces," Chem. Eng. Prog. Symp. Series, Vol. 56, #30, pp. 15-24 (1960).

7. Coury, G. E. and Dukler, A. E., "Turbulent Film Boiling on Vertical Surfaces: A Study Including the Influence of Interfacial Waves," 4th Intl. Heat Trans. Conf., Paper B3.6, Paris (1970).

8. Chi, J. W. H. and Vetere, A. M., "Two-Phase Flow During Transient Boiling of Hydrogen Determination of Nonequilibrium Vapour Fractions," Advan. Cryog. Eng., Vol. 9, pp. 243-253 (1964).

9. Chi, J. W. H., "Cooldown Temperatures and Cooldown Time During Mist Flow," Advan. Cryog. Eng., Vol. 10, pp. 330-340 (1965).

10. Chi, J. W. H., "Slug Flow and Film Boiling of Hydrogen," J. Spacecr. Rockets, Vol. 4, #10, pp. 1329-1332 (1967).

11. Kalinin, E. K., Koshkin, V. K., Yarkho, S. R., Berlin, I. I., Kochelaev, Y. S., Kostyuk, V. V., Kurolev, A. L., and Sdobnov, G. N., "Investigation of Film Boiling in Tubes with Subcooled Nitrogen Flow," 4th Intl. Heat Trans. Conf., Paper B.4.5, Paris (1970).

12. Laverty, W. F. and Rohsenow, W. M., "Film Boiling of Saturated Nitrogen Flowing in a Vertical Tube," ASME J. Heat Trans., Vol. 89, pp. 90-98 (1967).

13. Forslund, R. P. and Rohsenow, W. M., "Dispersed Flow Film Boiling," ASME J. Heat Trans., Vol. 90, pp. 399-407 (1968).

14. DeJarlais, G., "An Experimental Study of Inverted Annular Flow Hydrodynamics Utilizing an Adiabatic Simulation," ANL-83-44, NUREG/CR-3339 (1983).

15. DeJarlais, G., Ishii, M., and Linehan, J., "Hydrodynamic Stability of Inverted Annular Flow in an Adiabatic Simulation," Trans. ASME. J. Heat Trans., Vol. 108, pp. 84-92 (1986).

16. Ishii, M. and DeJarlais, G., "Flow Regime Transition and Interfacial Characteristics of Inverted Annular Flow," Nucl. Eng. Design, Vol. 95, pp. 171-184 (1986).

17. DeJarlais, G. and Ishii, M., "Inverted Annular Flow Experimental Study," ANL-85-31, NUREG/CR-4277 (1985).

18. Ishii, M. and DeJarlais, G., "Flow Visualization Study of Inverted Annular Flow of Post Dryout Heat Transfer Region," 3rd Intl. Topical Mtg. on Reactor Thermal Hydraulics, Paper 1.C, Newport, RI (1985).

19. Ishii, M. and DeJarlais, G., "Flow Visualization Study of Inverted Annular Flow of Post Dryout Heat Transfer Region," Nucl. Eng. Design, Vol. 99, pp. 187-199 (1987).

20. Graham, R. W., Hendricks, R. C., Hsu, Y. Y., and Friedman, R., "Experimental Heat Transfer and Pressure Drop of Film Boiling Liquid Hydrogen Flowing Through a Heated Tube," Advan. Cryog. Eng., Vol. 6, pp. 517-524 (1961).

21. Ottosen, P., "Experimental and Theoretical Investigation of Inverse Annular Film Flow and Dispersed Droplet Flow, Important Under LOCA Conditions," Riso National Laboratory Report No. R-424, Denmark (1980).

22. Kurilenko, A. A., Dymenko, S. R., and Kochelaev, Yu. S., "Phase Slip and Heat Transfer to the Liquid in Film Boiling of a Cryogenic Liquid in Piston Flow," J. Eng. Phys., Vol. 39, pp. 961-965 (1981).

23. Vojtek, I., "Investigation of Dispersed Flow Heat Transfer Using Different Computer Codes and Heat Transfer Correlations," The 1st Intl. Workshop on Fundamental Aspects of Post-Dryout Heat Trans., Salt Lake City, Utah, April 2-4, 1984, NUREG/CP-0060.

24. Webb, S. W. and Chen, J. C., "A Two-Region Vapor Generation Rate Model for Convective Film Boiling," The 1st Intl. Workshop on Fundamental Aspects of Post-Dryout Heat Trans., Salt Lake City, Utah, April 2-4, 1984, NUREG/CP-0060.

25. Groeneveld, D. C., "Inverted Annular and Low Quality Film Boiling: A State-of-the-Art Report," Keynote Paper, The 1st Intl. Workshop on Fundamental Aspects of Post-Dryout Heat Transfer, Salt Lake City, Utah, April 2-4, 1984, NUREG/CP-0060.

26. Chen, J. C., "Review of Post-Dryout Heat Transfer in Dispersed Two-Phase Flow," Keynote Paper, The 1st Intl. Workshop on Fundamental Aspects of Post-Dryout Heat Transfer, Salt Lake City, Utah, April 2-4, 1984, NUREG/CP-0060.

27. Yadigaroglu, G. and Bensalem, A., "Interfacial Mass Generation Rate Modeling in Non-Equilibrium Two-Phase Flow," Intl. Workshop on Two-Phase Flow Fundamentals, Gaithersburg, Maryland, Sept. 22-27, 1985.

28. Ishii, M. and Grolmes, M. A., "Inception Criteria for Droplet Entrainment in Two-Phase Concurrent Film Flow," AIChE J., Vol. 21, #2, pp. 308-317 (1975).

APPENDIX

EXPERIMENTAL DATA

This appendix is divided into four sections, the first two of which give test conditions for trials with nitrogen for α = 0.56 and 0.37, while conditions with helium and α = 0.37 are summarized in the third section. In each case, the data are tabulated under four main headings:

TRIAL RUN: A suffix lettering scheme, i.e., B, C, D, etc., is used to indicate trials for which numbers were not assigned previously.

TEMPERATURE, °C: T_g and T_f refer to gas and liquid temperatures, respectively.

DENSITY, kg/m^3: ρ_g = gas density evaluated using measured temperature and pressure via ideal gas law.
ρ_f = liquid density obtained from thermodynamic properties of "Freon" 113 by E.I. duPont Company

EXIT VELOCITY, m/s: V_g = average gas velocity at annulus
V_f = average liquid jet velocity

In the last section, the reduced data for the axial extent of the various flow regions are presented for selected trials. These are tabulated under the following column headings:

TRIAL RUN:

V_{rel}, m/s: Relative velocity defined as V_g - V_f.

L_B/D_j: Maximum nondimensional extent of each flow region.
A = smooth (small surface wave) section
B = rough wavy section
C = agitated section
D = dispersed (ligament and drop) section.

$(L_B/D_j)We_j^{-0.5}\ Re_j^{0.53}$: nondimensional groups, where Re_j and We_j are the liquid jet Reynolds and Weber numbers evaluated at the inlet to the test section. This is also divided into four columns, i.e., A, B, C, and D, the definition for each letter being exactly the same as given above.

$We_{g,rel}/\alpha^2$: gas Weber number scaled with the square of the void fraction (α).

Data for liquid surface tension are needed for computations of We_j and $We_{g,rel}$. The values used in the present analysis correspond to those reported by Sinitsyn et al. (1972).

REFERENCE

1. Sinitsyn, YE. N., Muratov, G. W., and Skripov, V. P., "The Surface Tension of F-11, 21 and 113," Heat Transfer-Soviet Research, Vol. 4, #4, p. 79 (1972).

A.I. Summary of Trials with Nitrogen and α = 0.56

Trial Run	Temperature, °C		Density, kg/m^3		Exit Velocity, m/s	
	T_g	T_f	ρ_g	$\rho_f \times 10^{-3}$	V_g	V_f
1	27	26	1.30	1.57	1.324	0.484
2	27	26	1.31	1.57	3.106	0.484
3	27	26	1.32	1.57	5.160	0.484
4	27	26	1.36	1.57	7.983	0.484
5	27	26	1.32	1.57	4.108	0.484
6	27	26	1.35	1.57	6.463	0.484
7	23	23	1.35	1.57	1.194	0.730
8	23	23	1.35	1.57	2.472	0.730
9	23	23	1.38	1.57	3.641	0.730
10	23	23	1.41	1.57	5.561	0.730
11	23	23	1.46	1.57	7.715	0.730
12	23	23	1.31	1.57	1.212	0.247
13	23	23	1.31	1.57	0.767	0.247
14	23	23	1.35	1.57	1.603	0.247
15	23	23	1.35	1.57	2.472	0.247
16	27	27	1.32	1.56	0.880	0.602
17	27	27	1.33	1.56	1.520	0.602
18	27	27	1.33	1.56	2.071	0.602
19	27	27	1.35	1.56	3.273	0.602
20	27	27	1.38	1.56	5.361	0.602
21	27	27	1.41	1.56	7.849	0.602
22	27	27	1.32	1.56	0.648	0.365
23	27	27	1.33	1.56	4.108	0.365
24	27	27	1.29	1.56	4.192	0.365
25	27	27	1.30	1.56	1.109	0.365
26	27	27	1.30	1.56	1.536	0.365
27	27	27	1.30	1.56	2.923	0.365
28	27	27	1.30	1.56	5.551	0.365
29	27	27	1.33	1.56	6.914	0.365
30	27	27	1.26	1.56	0.661	0.148
31	27	27	1.29	1.56	1.224	0.148

Trial Run	Temperature, °C		Density, kg/m^3		Exit Velocity, m/s	
	T_g	T_f	ρ_g	$\rho_f \times 10^{-3}$	V_g	V_f
32	27	27	1.29	1.56	1.645	0.148
33	27	27	1.27	1.56	2.538	0.148
34	27	27	1.26	1.56	2.973	0.148
35	27	27	1.27	1.56	3.791	0.148
36	27	27	1.29	1.56	3.774	0.247
37	27	27	1.30	1.56	5.511	0.247
38	27	27	1.36	1.56	0.865	0.730
39	27	27	1.29	1.56	0.655	0.098
40	27	27	1.30	1.56	0.994	0.098
41	27	27	1.29	1.56	1.336	0.098
42	27	27	1.29	1.56	1.645	0.098
43	27	27	1.29	1.56	2.121	0.098
44	27	26	1.37	1.57	5.628	0.730
45	27	26	1.33	1.57	6.513	0.484
46	27	26	1.29	1.57	0.777	0.247
47	27	26	1.27	1.57	0.660	0.098
48	27	26	1.24	1.57	2.154	0.098
49	27	26	1.25	1.57	2.772	0.098
50	27	26	1.25	1.57	3.407	0.098
51	27	26	1.29	1.57	0.656	0.074
52	27	26	1.29	1.57	0.997	0.074
53	27	26	1.27	1.57	1.339	0.074
54	27	26	1.27	1.57	1.653	0.074
55	27	26	1.25	1.57	2.138	0.074
56	27	26	1.25	1.57	2.772	0.074
57	27	26	1.25	1.57	3.390	0.074
58	27	26	1.25	1.57	4.225	0.074
59	27	26	1.27	1.57	5.261	0.074
60	27	26	1.35	1.57	1.607	0.730

A.II. Summary of Trials with Nitrogen and α = 0.37

Trial Run	Temperature, °C		Density, kg/m^3		Exit Velocity, m/s	
	T_g	T_f	ρ_g	$\rho_f \times 10^{-3}$	V_g	V_f
201	27	26	1.36	1.57	0.231	0.255
202	27	26	1.41	1.57	0.070	0.255
203	27	26	1.38	1.57	0.144	0.255
204	27	26	1.47	1.57	0.028	0.255
205	27	26	1.36	1.57	0.302	0.255
206	27	26	1.39	1.57	0.399	0.255
207	27	26	1.36	1.57	0.491	0.255
208	27	26	1.36	1.57	0.678	0.255
209	27	26	1.35	1.57	0.868	0.255
210	27	26	1.33	1.57	1.069	0.255
211	25	25	1.41	1.57	0.07	0.255
212	25	25	1.3[illegible]	1.57	0.302	0.255
213	25	25	1.31	1.57	1.253	0.255
214	25	25	1.34	1.57	0.072	0.052
215	25	25	1.41	1.57	0.028	0.052
216	25	25	1.33	1.57	0.145	0.052
217	25	25	1.31	1.57	0.236	0.052
218	25	25	1.31	1.57	0.309	0.052
219	25	25	1.29	1.57	0.414	0.052
220	25	25	1.31	1.57	0.501	0.052
221	25	25	1.29	1.57	0.698	0.052
222	25	25	1.29	1.57	0.892	0.052
223	25	25	1.27	1.57	1.181	0.052
224	25	25	1.26	1.57	1.528	0.052
225	25	25	1.26	1.57	2.188	0.052
226	25	25	1.26	1.57	3.874	0.052
227	26	26	1.32	1.57	0.070	0.255
228	26	26	1.35	1.57	0.3[illegible]	0.255
229	26	26	1.31	1.57	1.[illegible]	0.255
230	26	26	1.32	1.57	0[illegible]	0.052
231	26	26	1.29	1.57	0.3[illegible]	0.052

Trial Run	Temperature, °C		Density, kg/m^3		Exit Velocity, m/s	
	T_g	T_f	ρ_g	$\rho_f \times 10^{-3}$	V_g	V_f
232	26	26	1.27	1.57	1.273	0.052
233	26	26	1.24	1.57	5.160	0.052
234	26	26	1.42	1.57	0.227	0.510
235	26	26	1.40	1.57	0.399	0.510
236	26	26	1.40	1.57	0.668	0.510
237	26	26	1.37	1.57	0.964	0.510
238	26	26	1.36	1.57	1.228	0.510
239	26	26	1.37	1.57	0.072	0.069
240	26	26	1.40	1.57	0.028	0.069
241	26	26	1.35	1.57	0.232	0.069
242	26	26	1.33	1.57	0.307	0.069
243	26	26	1.31	1.57	0.499	0.069
244	26	26	1.31	1.57	0.693	0.069
245	26	26	1.28	1.57	0.892	0.069
246	26	26	1.27	1.57	1.182	0.069
247	26	26	1.27	1.57	1.448	0.069
248	26	26	1.27	1.57	1.770	0.069
249	28	28	1.20	1.56	0.324	0.052
250	28	28	1.21	1.56	1.301	0.052
251	28	28	1.27	1.56	0.150	0.052
252	28	28	1.30	1.56	0.074	0.069
253	28	28	1.25	1.56	0.316	0.069
254	28	28	1.25	1.56	0.904	0.069
255	28	28	1.31	1.56	0.074	0.103
256	28	28	1.31	1.56	0.499	0.103
257	28	28	1.31	1.56	0.521	0.510
258	28	28	1.31	1.56	2.071	0.510
259	28	28	1.31	1.56	3.173	0.510
260	28	28	1.33	1.56	4.375	0.510
261	28	28	1.38	1.56	5.511	0.510
262	28	28	1.38	1.56	8.150	0.510
263	28	28	1.36	1.56	0.072	0.103
264	28	28	1.39	1.56	0.028	0.103

Trial Run	Temperature, °C		Density, kg/m^3		Exit Velocity, m/s	
	T_g	T_f	ρ_g	$\rho_f \times 10^{-3}$	V_g	V_f
265	28	28	1.36	1.56	0.144	0.103
266	28	28	1.34	1.56	0.232	0.103
267	28	28	1.31	1.56	0.309	0.103
268	28	28	1.27	1.56	0.508	0.103
269	28	28	1.27	1.56	0.703	0.103
270	28	28	1.27	1.56	0.899	0.103
271	28	28	1.27	1.56	1.186	0.103
272	28	28	1.27	1.56	1.453	0.103
273	28	28	1.26	1.56	1.787	0.103
274	28	28	1.26	1.56	2.271	0.103
275	28	28	1.41	1.56	0.070	0.172
276	28	28	1.41	1.56	0.028	0.172
277	28	27	1.22	1.56	0.077	0.069
278	28	27	1.24	1.56	0.909	0.069
279	28	27	1.26	1.56	0.075	0.103
280	28	27	1.26	1.56	0.511	0.103
281	28	27	1.24	1.56	1.466	0.103
282	28	27	1.35	1.56	0.072	0.172
283	28	27	1.27	1.56	0.509	0.172
284	28	27	1.26	1.56	1.787	0.172
285	28	27	1.34	1.56	0.145	0.172
286	28	27	1.34	1.56	0.234	0.172
287	28	27	1.27	1.56	0.314	0.172
288	28	27	1.28	1.56	0.506	0.172
289	28	27	1.30	1.56	0.695	0.172
290	28	27	1.29	1.56	0.890	0.172
291	28	27	1.27	1.56	1.182	0.172
292	28	27	1.27	1.56	1.453	0.172
293	28	27	1.27	1.56	1.787	0.172
294	28	27	1.27	1.56	2.189	0.172
295	28	27	1.27	1.56	3.841	0.172
296	28	27	1.27	1.56	5.110	0.172
297	28	27	1.40	1.56	0.028	0.087

Trial Run	Temperature, °C		Density, kg/m^3		Exit Velocity, m/s	
	T_g	T_f	ρ_g	$\rho_f \times 10^{-3}$	V_g	V_f
298	28	27	1.31	1.56	0.074	0.087
299	28	27	1.31	1.56	0.309	0.087
300	28	27	1.27	1.56	0.701	0.087
301	28	27	1.25	1.56	1.186	0.087
302	28	27	1.24	1.56	1.887	0.087
303	28	27	1.41	1.56	0.028	0.137
304A	28	25	1.28	1.57	0.074	0.172
304B	28	25	1.28	1.57	0.506	0.172
305	28	25	1.27	1.57	1.770	0.172
306	28	25	1.36	1.57	0.023	0.137
307	28	25	1.34	1.57	0.074	0.137
308	28	25	1.31	1.57	0.309	0.137
309	28	25	1.29	1.57	0.696	0.137
310	28	25	1.27	1.57	1.182	0.137
311	28	25	1.27	1.57	1.870	0.137
312	28	25	1.26	1.57	2.522	0.137
313	28	25	1.26	1.57	4.810	0.137
314	28	25	1.36	1.57	0.072	0.337
315	28	25	1.38	1.57	0.229	0.337
316	28	25	1.38	1.57	0.403	0.337
317	28	25	1.34	1.57	0.596	0.337
318	27	27	1.38	1.56	0.072	0.337
319	27	27	1.36	1.56	0.231	0.337
320	27	27	1.35	1.56	0.304	0.337
321	27	27	1.35	1.56	0.406	0.337
322	27	27	1.35	1.56	0.595	0.337
323	27	27	1.33	1.56	0.788	0.337
324	27	27	1.32	1.56	1.071	0.337
325	27	27	1.32	1.56	1.336	0.337
326	27	27	1.32	1.56	1.587	0.337
327	27	27	1.32	1.56	1.921	0.337
328	27	27	1.31	1.56	2.405	0.337
329	27	27	1.31	1.56	4.409	0.337

Trial Run	Temperature, °C		Density, kg/m^3		Exit Velocity, m/s	
	T_g	T_f	ρ_g	$\rho_f \times 10^{-3}$	V_g	V_f
330	26	41	1.46	1.53	0.752	max.
331	30	36	1.30	1.54	0.074	0.337
332	30	36	1.29	1.54	0.416	0.337
333	30	36	1.24	1.54	0.075	0.103
334	30	35	1.20	1.55	0.030	0.052
335	30	35	1.25	1.55	0.421	0.103
336	30	36	1.29	1.54	0.416	0.337
337	30	37	1.31	1.54	0.074	0.337
338	26	36	1.32	1.54	0.074	0.337
339	26	36	1.32	1.54	0.234	0.337
340	26	37	1.31	1.54	0.413	0.337
341	26	37	1.30	1.54	0.606	0.337
342	26	36	1.31	1.54	0.795	0.337
343	26	37	1.30	1.54	1.079	0.337
344	26	35	1.32	1.55	0.074	0.103
345	26	35	1.31	1.55	0.236	0.103
346	26	34	1.27	1.55	0.418	0.103
347	26	37	1.38	1.54	0.072	0.337
348	26	34	1.29	1.55	1.349	0.337
349	26	35	1.27	1.55	1.870	0.337
350	26	35	1.28	1.55	2.355	0.337
351	26	37	1.29	1.54	3.824	0.337
352	26	36	1.31	1.54	5.043	0.337
353	26	37	1.38	1.54	0.072	0.510
354	26	37	1.42	1.54	0.227	0.510
355	26	38	1.37	1.54	0.403	0.510
356	26	38	1.46	1.54	0.0	0.510
357	27	39	1.38	1.53	0.072	0.510
358	27	40	1.33	1.53	0.234	0.510
359	27	40	1.32	1.53	0.074	0.337
360	27	41	1.30	1.53	0.236	0.337
361	27	41	1.31	1.53	0.501	0.337
362	27	41	1.32	1.53	0.030	0.255

Trial Run	Temperature, °C		Density, kg/m³		Exit Velocity, m/s	
	T_g	T_f	ρ_g	$\rho_f \times 10^{-3}$	V_g	V_f
363	27	41	1.29	1.53	0.237	0.255
364	27	41	1.29	1.53	0.030	0.172
365	27	40	1.29	1.53	0.149	0.172
366	27	41	1.30	1.53	0.414	0.172
367	27	39	1.29	1.53	0.030	0.069
368A	27	39	1.25	1.53	0.241	0.069
368B	27	41	1.43	1.53	0.070	0.421
369	23	38	1.41	1.54	0.070	0.421
370	23	39	1.36	1.53	0.234	0.421
371	23	40	1.33	1.53	0.60	0.421
372	23	40	1.33	1.53	1.336	0.421
373	23	38	1.27	1.54	0.075	0.052
374A	23	38	1.25	1.54	0.241	0.052
374B	23	40	1.39	1.53	0.072	0.337
374C	26	46	1.31	1.52	0.074	0.421
374D	26	46	1.34	1.52	0.241	0.172
375	25	15	1.33	1.59	0.977	0.337
376	25	17	1.33	1.59	0.234	0.103
377	25	17	1.27	1.59	1.359	0.103
378	25	16	1.24	1.59	0.075	0.052
379	25	15	1.33	1.59	0.074	0.052
380	25	15	1.33	1.59	0.074	0.052
381	25	15	1.28	1.59	0.239	0.103
382	25	15	1.28	1.59	0.239	0.103
383	25	15	1.26	1.59	1.363	0.103
384	25	15	1.26	1.59	1.363	0.103
385	25	15	1.34	1.59	0.974	0.337
386	25	15	1.25	1.59	0.075	0.052
387	25	15	1.26	1.59	0.241	0.103
388				UNASSIGNED		
389	25	15	1.26	1.59	1.363	0.103
390	25	15	1.33	1.59	0.980	0.337
391	25	15	1.23	1.59	0.075	0.052

Trial Run	Temperature, °C		Density, kg/m^3		Exit Velocity, m/s	
	T_g	T_f	ρ_g	$\rho_f \times 10^{-3}$	V_g	V_f
392	25	15	1.22	1.59	0.428	0.052
393	25	15	1.25	1.59	1.010	0.052
394	25	15	1.25	1.59	2.054	0.052
395	25	15	1.33	1.59	0.234	0.103
396	25	15	1.26	1.59	0.615	0.103
397	25	15	1.26	1.59	1.184	0.103
398	25	15	1.26	1.59	1.703	0.103
399	25	15	1.33	1.59	0.980	0.337
400	25	15	1.33	1.59	1.420	0.337
401	23	14	1.32	1.60	1.670	0.337
402	23	14	1.32	1.60	1.987	0.337
403	23	14	1.30	1.60	3.190	0.337
404	23	14	1.26	1.60	0.241	0.052
405	23	14	1.26	1.60	0.421	0.103
406	23	15	1.27	1.59	0.701	0.052
407	23	15	1.27	1.59	0.897	0.103
408	23	15	1.29	1.59	0.995	0.172
409	23	15	1.32	1.59	0.982	0.255
410	23	15	1.30	1.59	0.605	0.172
411	23	15	1.32	1.59	1.334	0.255
412	23	15	1.30	1.59	1.343	0.172
413	23	15	1.32	1.59	1.670	0.255
414	23	15	1.30	1.59	1.687	0.172
415	23	15	1.34	1.59	2.121	0.255
416	23	15	1.30	1.59	2.154	0.172
417	22	14	1.34	1.60	1.324	0.420
418	22	14	1.34	1.60	1.971	0.420
419	22	14	1.31	1.60	0.605	0.255
420	22	14	1.32	1.60	0.236	0.069
421	22	14	1.29	1.60	3.824	0.255
422	22	15	1.28	1.59	0.418	0.069
423	22	15	1.28	1.59	0.611	0.069
424	22	15	1.26	1.59	1.005	0.069

Trial Run	Temperature, °C		Density, kg/m^3		Exit Velocity, m/s	
	T_g	T	ρ_g	$\rho_f \times 10^{-3}$	V_g	V_f
425	22	15	1.26	1.59	1.366	0.069
426	22	15	1.26	1.59	1.703	0.069
427	22	15	1.28	1.59	1.268	0.103
428	22	15	1.27	1.59	2.271	0.069
429	22	15	1.28	1.59	1.703	0.103
430	22	[illegible]	1.26	1.59	2.288	0.069
431	22	15	1.26	1.59	1.703	0.069
432	22	15	1.27	1.59	1.002	0.069
433	22	15	1.26	1.59	0.421	0.069
434	22	35	1.34	1.55	2.121	0.421
435	22	35	1.30	1.55	0.606	0.255
436	22	35	1.29	1.55	1.171	0.255
437	22	35	1.28	1.55	0.805	0.172
438	22	35	1.29	1.55	1.687	0.255
439A	22	35	1.26	1.55	0.615	0.069
439B	22	35	1.29	1.55	2.171	0.255
439C	22	35	1.32	1.55	0.79	0.255
439D	22	35	1.35	1.55	0.406	0.421
439E	22	35	1.32	1.55	0.409	0.337
439F	22	35	1.34	1.55	0.232	0.337
440	22	23	1.40	1.57	0.229	0.421
441	22	23	1.37	1.57	0.403	0.421
442	22	23	1.36	1.57	0.680	0.421
443	22	23	1.36	1.57	0.969	0.421
444	22	23	1.34	1.57	1.324	0.421
445	22	23	1.34	1.57	1.974	0.421
446	22	23	1.34	1.57	0.074	0.069
447	22	23	1.36	1.57	0.232	0.069
448	22	23	1.33	1.57	0.496	0.069
449	22	23	1.29	1.57	0.888	0.069
450	22	23	1.44	1.57	0.070	0.172
451	22	23	1.37	1.57	0.302	0.172
452A	22	23	1.34	1.57	0.685	0.172
452B	22	23	1.32	1.57	1.159	0.172

A.III. Summary of Trials with Helium and α = 0.37

Trial Run	Temperature, °C		Density, kg/m^3		Exit Velocity, m/s	
	T_g	T_f	ρ_g	$\rho_f \times 10^{-3}$	V_g	V_f
700	22	24	0.189	1.57	0.222	0.103
701	22	24	0.199	1.57	0.074	0.103
702	22	24	0.180	1.57	0.878	0.103
703A	22	24	0.180	1.57	2.221	0.103
703B	22	24	0.189	1.57	0.222	0.103
703C	22	24	0.180	1.57	2.221	0.103
703D	22	24	0.189	1.57	0.222	0.103
703E	22	24	0.189	1.57	0.501	0.103
703F	22	24	0.189	1.57	0.222	0.103
704	24	24	0.181	1.57	1.620	0.172
705	24	24	0.186	1.57	0.626	0.172
706	24	24	0.182	1.57	1.107	0.172
707	24	24	0.181	1.57	2.655	0.172
708	24	24	0.181	1.57	4.041	0.172
709	24	24	0.186	1.57	0.224	0.052
710	24	24	0.190	1.57	0.075	0.052
711	24	24	0.181	1.57	1.111	0.052
712	24	24	0.179	1.57	0.882	0.052
713	24	24	0.177	1.57	2.238	0.052
714	24	24	0.186	1.57	0.867	0.255
715	24	24	0.183	1.57	2.204	0.255
716	24	25	0.182	1.57	0.227	0.069
717	24	25	0.184	1.57	0.077	0.069
718	24	25	0.179	1.57	0.506	0.069
719	24	25	0.177	1.57	0.888	0.069
720	24	25	0.177	1.57	1.820	0.069
721	24	25	0.175	1.57	2.672	0.069
722	24	25	0.186	1.57	0.035	0.069
723	24	25	0.179	1.57	0.506	0.103
724	24	25	0.178	1.57	1.359	0.103
725	24	25	0.192	1.57	0.035	0.052

Trial Run	Temperature, °C		Density, kg/m^3		Exit Velocity, m/s	
	T_g	T_f	ρ_g	$\rho_f \times 10^{-3}$	V_g	V_f
726	24	25	0.175	1.57	1.368	0.052
727	24	25	0.198	1.57	0.189	0.172
728	24	25	0.195	1.57	0.219	0.255
729	24	25	0.183	1.57	1.338	0.255
730	24	25	0.188	1.57	0.860	0.337
731	24	25	0.201	1.57	0.033	0.337

A.IV. Axial Extent of Various Flow Regimes for Selected Trials

Trial Run	V_{rel} (m/s)	L_B/D_j				$(L_B/D_j)\ We_j^{-0.5}\ Re_j^{0.53}$				$We_{g,rel}/\alpha^2$
		A[1]	B[2]	C[3]	D[4]	A	B	C	D	
234	-0.283	38.9	60.2			371	573	-		0.50
236	0.158	5.6	37.0	88+		53	352	1023+		0.16
237	0.454	3.2	23.2	88+		31	221	1023+		1.30
238	0.720	2.8	20.4	88+		27	194	1023+		3.30
239	0.003	4.6	13.9	27.8		113	339	678		0.6×10^{-4}
240	-0.041	5.6	15.7	27.8		136	385	678		0.01
241	0.163	4.6	13.9	37.0		113	339	903		0.16
242	0.238	1.9	11.1	32.4		45	271	790		0.34
243	0.430	1.4	11.1	32.4		34	271	790		1.11
244	0.624	0.9	10.2	32.4		23	248	790		2.34
245	0.823	0.5	7.4	26.0		11	181	632		4.1
246	1.10	0.5	2.8	23.2		11	68	565		7.4
247	1.374	0.5	2.8	18.5		11	68	452		11.6
248	1.70	0	0	13.9		0	0	339		17.6
257	1.160	1.9	14.8	69.4	88+	18	141	807	837+	8.5
258	1.560	1.4	14.8	60.2	88+	13	141	700	837+	15.3
259	2.660	0.9	11.1	55.6	88+	8	106	647	837+	44.6
260	3.870	0.9	7.4	32.4	88+	8	71	377	837+	94.3
261	5.0	0.9	7.4	18.5	88	8	71	215	837	157.4

1 = smooth solid core, 2 = rough wavy section, 3 = agitated section, 4 = dispersed section.
+ Region extends beyond heated portion of test section.

Trial Run	V_{rel} (m/s)	L_B/D_j				$(L_B/D_j)\ We_j^{-0.5}\ Re_j^{0.53}$				$We_{g,rel}/\alpha^2$
		A^1	B^2	C^3	D^4	A	B	C	D	
262	7.640	0.9	5.6	13.9	64.8	8	53	162	617	367.6
275	-0.102	11.1	25.9	55.6		176	412	882		0.063
276	-0.144	11.1	20.4	37.0		176	323	589		0.13
278										
285	-0.03	6.5	18.5	45.3		103	294	735		0.0054
286	0.058	4.6	23.2	50.9		74	367	808		0.02
287	0.142	1.9	14.8	50.9		29	235	808		0.12
288	0.338	0.9	11.1	45.3		15	176	735		0.69
289	0.523	0.5	11.1	45.3		7	176	735		1.65
290	0.718	0.5	5.6	45.3		7	88	735		3.11
291	1.008	0.9	11.1	37.0		15	176	588		6.14
292	1.278	0.9	5.6	27.8		15	88	441		9.9
293	1.578	0.9	3.7	27.8		15	59	441		15.1
294	2.018	0.5	5.6	27.8		7	88	441		24.6
295	3.668	0.5	-	9.3		7	-	147		81.3
296	4.938	0.5	-	7.4		7	-	118		147.4
314	-0.266	25.0	41.7	88+		290	485	1023		0.44
315	-0.109	18.5	46.3	83.3	88+	215	538	969	1023+	0.074
316	0.065	9.3	32.4	74.1	88+	108	377	862	1023+	0.0026
317	0.258	2.8	27.8	60.2	88+	32	323	700	1023+	0.412
318	-0.266	27.8	50.9	88+		323	592	1023		0.44

1 = smooth solid core, 2 = rough wavy section, 3 = agitated section, 4 = dispersed section.
+ Region extends beyond heated portion of test section.

Trial Run	V_{rel} (m/s)	L_B/D_j				$(L_B/D_j)\ We_j^{-0.5}\ Re_j^{0.53}$				$We_{g,rel}/\alpha^2$
		A[1]	B[2]	C[3]	D[4]	A	B	C	D	
319	-0.107	23.2	41.7	88+		270	485	1023		0.071
320	-0.034	18.5	41.7	83.3		215	485	969	1023+	0.007
321	0.068	5.6	32.4	78.7		65	377	915	1023+	0.029
322	0.257	3.7	32.4	64.8		43	377	754	1023+	0.41
323	0.450	1.9	23.2	64.8		22	270	754	1023+	1.25
324	0.733	1.4	14.8	60.2		16	172	700	1023+	3.32
325	0.998	0.9	11.1	55.6	88+	11	129	647	1023+	6.2
326	1.249	0.9	9.3	46.3	83.3	11	108	538	965	9.7
327	1.583	0.5	4.6	29.6	88	5	54	344	1023	15.5
328	2.061	0.9	4.6	23.2	83.3	11	54	270	965	26.4
329	4.071	0.9	4.6	9.3	69.4	11	54	108	807	103.1
704	1.448	0.9	9.3	44.4		15	147	706		1.8
705	0.458	4.6	23.2	50.9		74	367	808		0.18
706	0.938	1.1	19.4	50.9		18	309	808		0.76
707	2.488	0.9	6.5	41.7		15	103	661		5.31
708	3.868	0.7	3.7	23.2		10	59	367		12.83
716	0.117	3.2	14.8	25.9		79	361	632		0.011
717	0.008	3.7	16.7	29.6		90	407	723		0.5×10^{-4}
718	0.437	0.9	13.9	29.6		23	339	723		0.16
719	0.819	0.9	10.2	25.0		23	248	610		0.56
720	1.750	0.5	6.5	23.2		11	158	565		2.53
721	2.60	0.5	4.6	18.5		11	113	452		5.59

1 = smooth solid core, 2 = rough wavy section, 3 = agitated section, 4 = dispersed section.
+ Region extends beyond heated portion of test section.

Trial Run	V_{rel} (m/s)	L_B/D_j				$(L_B/D_j)\ We_j^{-0.5}\ Re_j^{0.53}$				$We_{g,rel}/\alpha^2$
		A[1]	B[2]	C[3]	D[4]	A	B	C	D	
722	-0.034	7.4	20.4	35.2		181	497	858		0.001
727	0.017	5.6	25.9	50.9		79	412	808		0.0003
730	0.522	1.4	20.4	69.4	88+	16	237	807	1023+	0.24
731	-0.306	29.6	55.6	88		344	647	1023	-	0.081
742	-0.118	9.3	46.3	78.7	88+	108	538	915	1023+	0.012
746	0.530	1.4	23.2	60.2	88+	16	270	700	1023+	0.24
781	5.222	1.4	5.6	9.3	69.4	16	65	108	807	23.7
782	-0.118	16.7	44.4	83.3	88+	194	516	909	1023+	0.012
783	0.156	4.6	32.4	78.7	88+	54	377	915	1023+	0.021
784	1.432	1.9	16.7	60.2	83.3	22	194	700	964	1.8
785	2.267	0.9	5.6	41.7	74.1	11	65	485	861	4.5
786	4.004	0.9	5.6	20.4	69.4	11	65	237	807	13.9

1 = smooth solid core, 2 = rough wavy section, 3 = agitated section, 4 = dispersed section.
+ Region extends beyond heated portion of test section.

Distribution for NUREG/CR-4972 (ANL-87-27)

Internal:

C. E. Till	W. T. Sha	Y. S. Cha
J. F. Marchaterre	Y. W. Shin	A. C. Raptis
A. J. Goldman	J. Sienicki	M. Ishii (17)
L. W. Deitrich	D. W. Condiff	ANL Patent Dept.
D. Rose	S. Y. Lee	ANL Contract File
D. H. Cho	M. Tang	ANL Libraries
B. W. Spencer	N. T. Obot (6)	TIS Files (5)

External:

USNRC Washington, for distribution per R2 and R4 (325)
DOE-TIC (2)
Manager, Chicago Operations Office
Reactor Analysis and Safety Division Review Committee:
- W. B. Behnke, Jr., Commonwealth Edison Co., Chicago, Ill. 60690
- M. J. Ohanian, Univ. of Florida, Gainesville, Fla. 32611
- R. L. Seale, Univ. of Arizona, Tucson, Ariz. 85721
- J. S. Armijo, General Electric Company, San Jose, Calif. 95153-5354
- T. J. Hirons, Los Alamos National Laboratory, Los Alamos, N. Mex. 87545
- N. E. Todreas, Mass. Inst. of Technology, Cambridge, Mass. 02139

A. E. Dukler, Univ. of Houston, Tex. 77004
O. C. Jones, Rensselaer Polytechnic Inst., Troy, N. Y. 12181
G. Kocamustafaogullari, Univ. of Wisconsin-Milwaukee, Milwaukee, Wis. 53201
K. A. Williams, Science Applications International, Albuquerque, N. Mex. 87102

NRC FORM 335 (2-84) NRCM 1102, 3201, 3202

U.S. NUCLEAR REGULATORY COMMISSION

BIBLIOGRAPHIC DATA SHEET

SEE INSTRUCTIONS ON THE REVERSE

1. REPORT NUMBER (Assigned by TIDC, add Vol. No., if any)
NUREG/CR-4972
ANL-87-27

2. TITLE AND SUBTITLE
TWO-PHASE FLOW REGIME TRANSITION CRITERIA IN POST-DRYOUT REGION BASED ON FLOW VISUALIZATION EXPERIMENTS

3. LEAVE BLANK

4. DATE REPORT COMPLETED

MONTH	YEAR
June	1987

5. AUTHOR(S)
N. T. Obot and M. Ishii

6. DATE REPORT ISSUED

MONTH	YEAR
June	1987

7. PERFORMING ORGANIZATION NAME AND MAILING ADDRESS (Include Zip Code)
Reactor Analysis and Safety Division
Argonne National Laboratory
9700 S. Cass Avenue
Argonne, Illinois 60439

8. PROJECT/TASK/WORK UNIT NUMBER

9. FIN OR GRANT NUMBER
A2026

10. SPONSORING ORGANIZATION NAME AND MAILING ADDRESS (Include Zip Code)
Reactor Systems Branch
Division of Reactor System Safety
Office of Nuclear Regulatory Research
U.S. Nuclear Regulatory Commission
Washington, D.C. 20555

11a. TYPE OF REPORT
Technical

b. PERIOD COVERED (Inclusive dates)
June 1986 - May 1987

12. SUPPLEMENTARY NOTES

13. ABSTRACT (200 words or less)

A visual study of film boiling using photographic and high speed motion-picture methods was carried out to determine the flow regime transition criteria in the post CHF region. An idealized inverted annular flow was obtained by introducing a liquid jet of Freon 113 through a nozzle, precisionly centered with respect to the internal diameter of the test section, with an annular gas flow. The respective ranges for liquid and gas exit velocities were 0.05-0.5 and 0.03-7.9 m/s. Nitrogen and helium were used in the study.

For the present configuration, there are four basic flow regimes. Beginning from the nozzle exit, there is a smooth, inverted annular flow section with liquid in the core and gas in the annulus; followed by the rough wavy section with an intact liquid core, the agitated and the dispersed flow regimes. For a given liquid jet velocity, the axial extent of each flow regime decreases with increasing gas velocity through the annulus.

Generalized transition criteria and simplified correlations for the axial limits of the various flow regimes have been developed, by extending the results of previous studies on adiabatic inverted annular flow.

14. DOCUMENT ANALYSIS - a. KEYWORDS/DESCRIPTORS

Film Boiling
Inverted Annular Flow
Two-phase Flow
Post-CHF Hydrodynamics
Core Reflooding
Flow Regime
Droplet Size
Jet Disintegration
Interfacial Instability

b. IDENTIFIERS/OPEN-ENDED TERMS

15. AVAILABILITY STATEMENT
Unlimited

16. SECURITY CLASSIFICATION
(This page)
Unclassified
(This report)
Unclassified

17. NUMBER OF PAGES

18. PRICE

120555078877 1 1AN1R21R4
US NRC-OARM-ADM
DIV OF PUB SVCS
POLICY & PUB MGT BR-PDR NUREG
W-537
WASHINGTON DC 20555